© 2015 IJSRST | Volume 1 | Issue 5 | Print ISSN: 2395-6011 | Online ISSN: 2395-602X
Themed Section: Science and Technology

Assessment of the Relationship between Actual Evapotranspiration, Reference Evapotranspiration and Precipitation (A case study of Tono Irrigation Scheme)

Adams Sadick[*1], Ekow Gaisie[2], Eric Owusu Adjei[3], Kennedy Agyeman[4], Kwabena A. Nketia[5], Eric Asamoah[6]

*[1]Soil Chemistry and Mineralogy, Soil Research Institute, Kumasi, Ghana
[2]Soil and Water Conservation, Soil Research Institute, Kumasi, Ghana
[3]Directorate, Soil Research Institute, Kumasi, Ghana
[4]Resource and Crop Management, Crops Research Institute, Kumasi, Ghana
[5,6] Soil Genesis, Survey and Survey Division, Soil Research Institute, Kumasi, Ghana

ABSTRACT

The study was carried out to assess the relationship between actual evapotranspiration, reference evapotranspiration and precipitation in the effect of optimum planting date of crops in the Tono irrigation area. The Surface Energy Balance System (SEBS) and Penman Monteith method were used to estimate actual and reference evapotranspiration and other energy fluxes in the monthly and seasonal time steps using climatic parameters. The rainfall data was obtained from the office of meteorological station in Navrongo, Ghana. The study showed that at the peak of the rainy season where there is abundant of moisture in the soil, ET_a rate equals ET_o. When the moisture content in the soil is limited as a result of insufficient rainfall and the crops unable to absorb water from the soil, the ET_a becomes lower than ET_o. Precipitation was much higher than ET_o in the month of April which was the optimum planting date of most crops and October.

Keywords: Evapotranspiration, Hydrological Cycle, Irrigation, Geographical Information System, Remote Sensing

I. INTRODUCTION

The evapotranspiration (ET), which involves water evaporation from soil surfaces and vegetation transpiration, represents a fundamental development of hydrological cycle and is a key element of water resources management, particularly in semi-arid and arid regions (Budyko, 1974; Bouwer et al., 2008). Some studies have demonstrated that the temporal and spatial patterns of ET depend on a large variety of influencing factors like vegetation and soil types, topography, and the meteorological conditions (Milly and Dunne, 2001; Gordon et al., 2003; Bouwer et al., 2008). The primary methods used conventionally to measure ET are dependent of the field or landscape scales (Bowen ratio, eddy covariance, soil water balance), but do not allow the evaluation of fluxes when dealing with larger spatial scales due to the inherent heterogeneity of land surfaces and the dynamic nature of water vapor transport processes (Gao et al., 2008).

The quantification of the ET losses on a regional scale and in high spatial resolution is an essential element for hydrological modeling, analysis of the water use on basin scale and adoption of correct irrigation management. Nowadays, with the increasing resolution of the satellite imagery, remote sensing techniques provides parameters at various temporal and spatial scales required to estimate actual evapotranspiration (ET_a). Surface Energy Balance System (SEBS) (Su et al., 2001) uses spectral radiance recorded by satellite sensors and meteorological data to obtain the surface energy balance at regional scale.

The Penman-Monteith method as modified by Allen (1986) is the most accurate method to estimate potential evapotranspiration. Because of its accuracy, the Penman-Monteith method is used since temperature, relative humidity, wind speed sunshine hours data are available in the study area. Reference crop evapotranspiration (ET_o) has to be estimated in daily time step by step using Penman-Monteith method (recommended by the FAO). The reference evapotranspiration (ETo) represents the potential evapotranspiration of a well-watered grass crop with an assumed height of 0.12m, a fixed surface resistance of 70s/m and an albedo of 0.23 (Allen et al. 1986).

The aim of this study was to evaluate the relationship between actual evapotranspiration, reference evapotranspiration and precipitation in the effect of optimum planting date of crops in the study area.

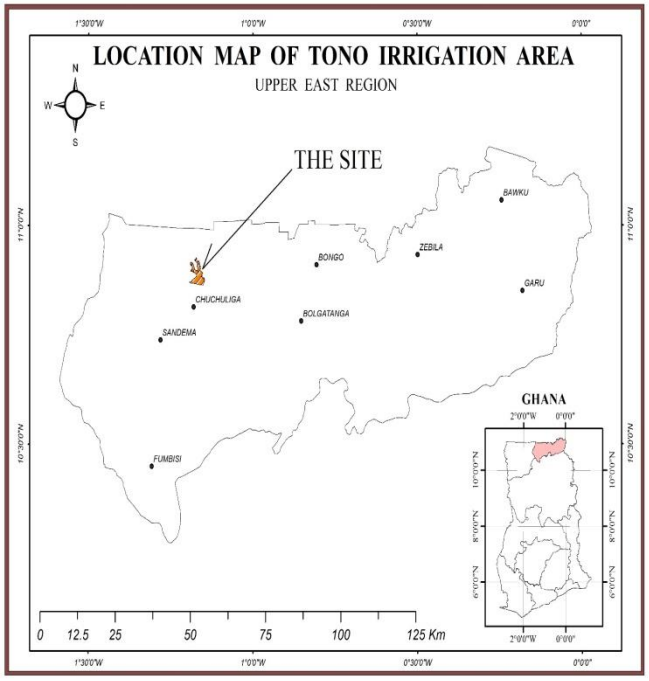

Figure 1: Map of Ghana showing Tono Irrigation Area

II. METHODS AND MATERIAL

The study was conducted in the Tono irrigation area which lies in the guinea savannah agro-ecological zone of Ghana, and it is located in the Upper East Region and lying between latitude 10 ^{o} 45$^{'}$ N and longitude 1^{o} 0$^{'}$ W. It has a potential area of about 3,840 ha with a developed area of about 3,450 ha. The project area comprises eight (8) command areas, namely Bonia, Gaani, Korania, Wuru, Yigania, Yigwania, and Chuchuliga zone A and B. The major crops cultivated in this area are rice, maize, cowpea, tomato, pepper and onion, with maize having the highest cultivated area.

The total annual rainfall in the area is around 950mm which normally begins in May, reach a peak in August then drop sharply in October. Thereafter, there is a long dry period from November to the end of April during which period only negligible amounts of rain are received.

Mean monthly temperatures remain high throughout the year only falling around 26^{o}C in August and September at Navrongo. March and April are the hottest months recording nearly 32^{o}C. Absolute minimum temperatures of around 16^{o}C are usually recorded in December or January with absolute maximum temperature of about 35^{o}C recorded in March and April.

Relative humidity percent for the study area is high during rainy season in particular, from July to September, and low in the dry (harmattan) period from January to February. Detailed data indicate low diurnal and monthly humidity readings between noon (12:00) and 15:00 hours and high diurnal humidity readings between midnight and 06:00 hours. Usually, humidity during the noon to 15:00 hours period may be 20 to 30 percent lower than at 09:00 hours.

During the fieldwork campaign for data collection, it was observed that the survey area falls within the elevation range 505–620ft above sea level. The topography is generally nearly level (0-2%) to gently

sloping (2-5%). Steeper slopes of between 5-9% occur occasionally on isolated hills and inselbergs. Owing to the generally low relief, surface runoff is slow but along the gentle slopes runoff has caused moderate to slight erosion. A number of extensive depressions are seen throughout the area. These become waterlogged or flooded during wet seasons but become dry in the alternate dry season.

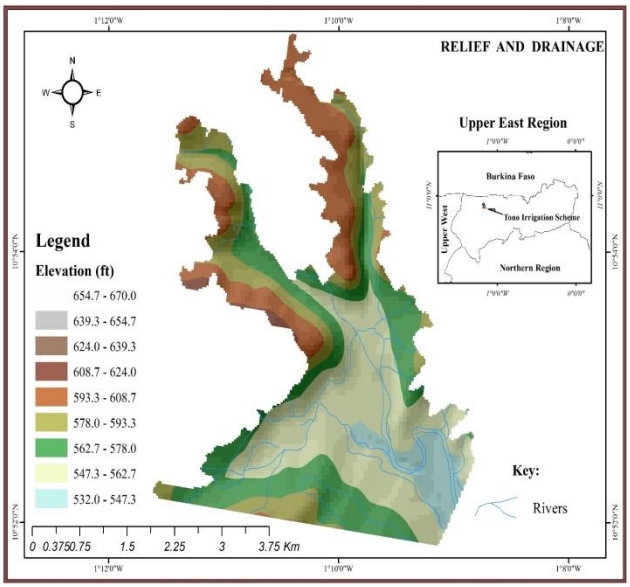

Figure 2: Map showing Relief and Drainage for Tono Irrigation Area

The original tree-savannah vegetation of the area has been largely destroyed by farming activities most of the trees being felled for firewood and building construction. *Batyrespernum parkii* (shea butter tree) is the dominant economic tree species, while Teak, an exotic plant, occurs scattered throughout the area. Other existing trees include *Diospyrus mespillferais, Perkia filicoidia* (dawadawa tree), *Adansonia digitata* (baobah tree), *Anogeissus leocarpus, Vitex cionkowskii, Entanda abyssinica, Sterculia tomontosa, Bombax buonopozense, Balanites aegyptinca* and Ficus species. Of the grasses, *Aristidakerstingii, Heteropogoncontotus* and *Eragrestis* species are dominant and occur in association with few medium and tall grasses including *Penisetuapediselatum, Rotboeliaoxaltata* and *Hyparrheniarufa*

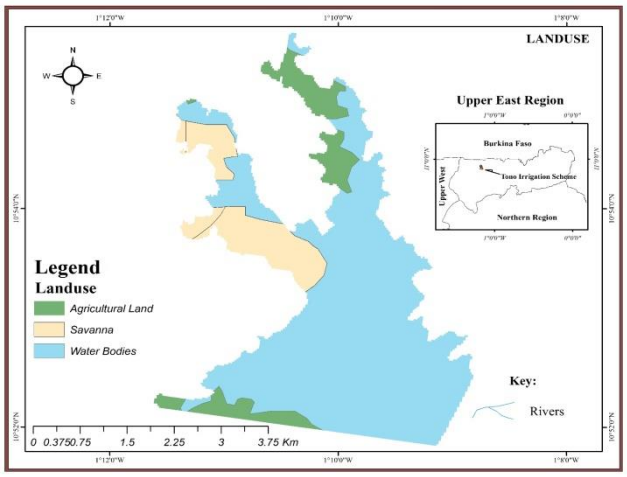

Figure 3: Map showing Relief and Drainage for Tono Irrigation Area

Data Acquisition

Climatological data such as rainfall, temperature, windspeed, sunshine and humidity were collected from meteorological station located inside the study area for the estimation of effective precipitation and evapotranspiration.

USDA Soil Conservation Service method was used to estimate the effective rainfall as follows (Smith, 1991):

$$P_{eff} = P_{tot} \times \frac{125 - 0.2P_{tot}}{125} \quad \text{For } P_{tot} < 250\text{mm}$$

$$P_{eff} = 125 + 0.1P_{tot} \quad \text{For } P_{tot} > 250\text{mm}$$

Where P_{eff} = Effective rainfall

P_{tot} = Total rainfall

Estimation of Actual Evapotranspiration using Surface Energy Balance System (SEBS) Algorithm

Twelve aster images of DOY (day of the year): 16, 47, 75, 106, 136, 167, 197, 228, 259, 289, 320 and 350 of the study area were downloaded from the website (http://earthexplorer.usgs.gov). These were used with SEBS covering the two seasons of the year (2009).

The remote sensing input used for this study is Aster data having the description in table 1 below.

Description of coordinate systems used in all of the maps and images in this study is as follows:

Projection: UTM
Datum: WGS 84

The Surface Energy Balance System (SEBS) by Su et al., (2001) was used to estimate actual evapotranspiration (ET_a) and other energy fluxes in daily, monthly and seasonal time steps. Estimation of ET_a is the most crucial part in the study of irrigation performance (Adams et al. 2014). The SEBS is the process of estimating ET_a and other energy fluxes based on remotely sensed data from satellites. Because the process uses satellite images of different dates, the major advantage of the process is that ET_a can be computed over large areas in different times (Su et al. 2001)

The SEBS procedure by Su et al. (2001), consists of three main processes: Image import, Pre-processing and Direct SEBS algorithm application. The area under study was a flat plane therefore Aster level-1B was downloaded and import in ILWIS. The pre-processing involves the following steps:

- Geometry parameters such as inclination, solar azimuth angle, zenith angle, solar elevation, date of the image of all the bands from HDF file.
- Estimation of radiance from some of the above parameters
- Converting radiance to reflectance(at sensor)
- Atmospheric correction of visible(VIS) and near infrared(NIR) bands using Simplified Method for the Atmospheric Correction (SMAC)
- Land surface albedo computation
- Land surface emissivity computation
- Brightness temperature computation
- Land surface temperature computation

The radiance, which the radiative energy in a given direction per unit time per unit wavelength range per unit solid angle per unit area perpendicular to a given direction, of each band was computed using the relation:

$$Rad = Inc. \times DN + Offset$$

Where Inc. = Inclination and DN = Digital number

A. Radiance to Reflectance (at sensor)

Once the radiance is obtained, the reflectance at the sensor is computed using visible and shortwave infrared bands. Here, solar zenith angle (31.09^o) is required as input parameter. The equation for at-sensor reflectance is expressed as follows:

$$R_{TOA} = \frac{\pi \times L_{sat} \times d^2}{ESUN_{\lambda} \times Cos\,\theta_s}$$

Where R_{TOA}= At-sensor reflectance (top-of-atmosphere reflectance), L_{sat}= at-sensor radiance, d= earth-sun distance calculated using the equation below:

$$d = \left[1 - 0.01672 \times Cos\left(0.9856 \times \left(julianday - 4\right)\right)\frac{3.14159}{180}\right]$$

$ESUN_{\lambda}$= the in-band solar constant which is different from ASTER band. This constant is given in the header file and Aster documentation. It is the solar irradiance emitted by the sun at the top of the atmosphere for the wavelength range of each band and θ_s= solar zenith angle which is also given by: 90^o-Solar elevation angle. The solar elevation angle was obtained from the ASTER metadata file.

B. Brightness Temperature Computation

Brightness temperature, Tc**,** is defined as the temperature of a blackbody that emits the same intensity as measured at a given wavelength (or frequency or wave number). In this computation, the procedure provides option to convert the bands 13 and 14 of ASTER from radiances to blackbody temperature, using the Planck equation as follows:

$$T_c = \frac{C_2}{\lambda_c \log\left(\frac{C_1}{\lambda_c^5 \times \pi \times L_s} + 1\right)}$$

Where T_c= the brightness temperature from central wavelength and λ_c= the sensor's central wavelength

C. Atmospheric Correction (SMAC)

SMAC was used as a tool for the atmospheric effect correction of the visible and near visible bands of the ASTER image. The algorithm by Rahman, H and Dedieu G., 1994 is used. SMAC requires information of the atmospheric composition at the moment the satellite passes and information of the geometry of the satellite and sun. The set of inputs required by SMAC is listed below:

Top atmospheric reflectance channel and coefficient file for sensor which were calculated above, optical

thickness (nm), water vapour content (gm^{-2}) and ozone content (atm.cm) which were also obtained from the site (http://aeronet.gsfc.nasa.gov) and the surface pressure from meteorological station closed to the study area. The solar zenith angle and azimuth angle were obtained from ASTER metadata file.

D. Land Surface Albedo Computation

The surface albedo was computed using reflectance bands 1, 3, 5, 6, 8 and 9. The reflectance bands 5, 6, 8 and 9 need to be resampled first before the surface albedo computation because of incompatibilities in the georeference. The formula by Liang et al., 2000 was used in this case to compute surface albedo.

E. Land Surface Emissivity Computation

The surface emissivity was estimated using the atmospherically corrected surface reflectance in the red (VIS2) and near infrared (NIR3) bands, and this method is restricted to land pixels. The method used in estimating the land surface emissivity was formulated by Valor and Caselles (1996) as:

$$\varepsilon_o = \varepsilon_c f_c + \varepsilon_s (1 - f_c) + 4(d\varepsilon) f_c (1 - f_c)$$

Where ε_c is emissivity of full vegetation cover, ε_s emissivity of bare soil, f_c the fractional vegetation cover, $d\varepsilon$, the vegetation structure parameter. According to Valor and Caselles (1996) ε_c, εs and $d\varepsilon$ are taken as 0.985, 0.96 and 0.015 respectively. The fractional vegetation cover is derived in the SEBS algorithm below. The NDVI are indicators of photosynthetic activity at the vegetation surface. Because of the strong spectral absorption of chlorophyll in the visible region and the high reflectance of vegetation in the NIR part, the reflectance value in these bands is used to provide the information of the vegetation status. The NDVI values will be calculated with the equation based on the atmospherically corrected surface reflectance:

$$NDVI = \frac{NIR3N - VIS2}{NIR3N + VIS2}$$

F. Land Surface Temperature Computation

This was computed by correcting the georeference of the brightness temperature maps of band 13 and 14 to get the same georeference in the visible bands.

The following information from remote sensing data is required by SEBS algorithms, which have been determined above: the land surface albedo, emissivity, NDVI and temperature. These parameters are to be determined first. Secondly, the meteorological inputs required by SEBS are also specific humidity (kg/kg), wind speed (m/s), air temperature (°C), air pressure (Pa), sunshine hours and solar radiation. Thirdly, fractional vegetation covers, leaf area index, surface roughness for momentum transport and roughness length for heat transport are also to be used as input parameters.

Estimation of input Parameters for SEBS

A. Fractional Vegetation Cover

The fraction vegetation cover is used to break up non-vegetated, partially vegetated and densely vegetated land surfaces. This parameter was used in SEBS model to derive surface temperature as indicated above, LAI and ground heat flux. This can be determined from remote sensing data. The formula by Choudhory et al., 1994 was applied to determine the parameter as:

$$f_c = 1 - \left[\frac{NDVI_{\max} - NDVI}{NDVI_{\max} - NDVI_{\min}} \right]^p$$

The exponential P represent the ratio of the leaf angle distribution and taken as 0.625
$NDVI_{max}$ is the NDVI value of the full vegetation cover
$NDVI_{mim}$ is the NDVI value of bare soil and
NDVI is the value of the current pixel

B. Leaf Area Index

The leaf area index is defined as the one sided green leaf area per unit ground area of the canopies. Typical values of LAI for a variety of land covers are crucial for proper model of satellite based on energy balance modeling for a specific area. For this study the exponential relationship formulated by Choudhury (1987) is used as:

$$LAI = \log \frac{(1 - f_c)}{-\Lambda}$$

Where f_c is fractional canopy cover and Л the leaf angle distribution function.

In SEBS, this parameter is applied in the determination of the roughness height for heat transfer (Z_{oh})

C. Surface Roughness Height for Momentum Transport

The roughness height for momentum transfer is used as reference height for momentum flux calculation. The empirical formula by Su et al., (2001) used as:

$$Z_{om} = 0.005 + 0.5\left[\frac{NDVI}{NDVI_{\max}}\right]^{2.5}$$

D. Roughness Length for Heat Transfer

The scalar roughness height for heat transfer is computed as:

$$Z_{oh} = \frac{Z_{om}}{\exp(KB^{-1})}$$

Where KB^{-1} is excess resistance for heat transfer. The KB^{-1} is used to compare Z_{om} and $Z_{oh.}$ Moreover, the determination of KB^{-1} is based on Su et al., (2001) physical model as:

$$KB^{-1} = \frac{KC_d}{4C_t \frac{u_*}{u(h)}\left(1 - e^{\frac{-nec}{2}}\right)} f_c^2 + 2 f_c f_s \frac{K \times \frac{u*}{u(h)}}{C_t^*} + KB_s^{-1} f_s^2$$

Where f_c is the fractional canopy coverage and f_s its compliment. C_t is the heat transfer coefficient of the leaf. For most canopies and environmental conditions, C_t is between 0.005N and 0.075N (N is number of sides of a leaf to participate in heat exchange). C_d is the drag coefficient of the foliage.

Similarity Theory

According to Brutsaert (1999), this refers to the principle of properly scaling a specific physical phenomenon to get a universal relationship between them. The Monin-Obukhov similarity theory is applied to derive the friction velocity, sensible heat flux and stability length as follows:

$$U = \frac{u_*}{K}\left[In\left(\frac{Z - d_o}{Z_{om}}\right) - \psi_m\left(\frac{Z - d_o}{L}\right) + \psi_m\left(\frac{Z_{om}}{L}\right)\right]$$

$$\theta_o - \theta = \frac{H}{k u_* \rho C_p}\left[In\left(\frac{Z - d_o}{Z_{oh}}\right) - \psi_h\left(\frac{Z - d_o}{L}\right) + \psi_h\left(\frac{Z_{oh}}{L}\right)\right]$$

Where Z is the reference height above the surface, u_* is the friction velocity, ρ is the density of air, k= 0.4 von Karman's constant, d_o is the zero displacement height, Z_{om} is the roughness height for momentum transfer, Z_{oh} is roughness length for heat transport, θ_o and θ_a are the potential temperature at the surface and air, Ψ_m and Ψ_h are stability correction functions for momentum and sensible heat transfer. The Obukhov length L, is expressed as:

$$L = \frac{\rho C_p u_*^3 \theta_v}{kgH}$$

Where g is the acceleration due to gravity and θ_v is the potential virtual temperature near the surface.

Land Surface Heat Flux Estimation

A. Net Radiation

The energy balance equation which governs the SEBS process is mathematically expressed as:

$$R_n = \lambda E + G + H$$

Where R_n, the net radiation,(Wm^{-2}), λE, the latent heat flux(λ is the latent heat of vaporization and E is the actual evapotranspiration), G is soil heat flux and H is the sensible heat flux.

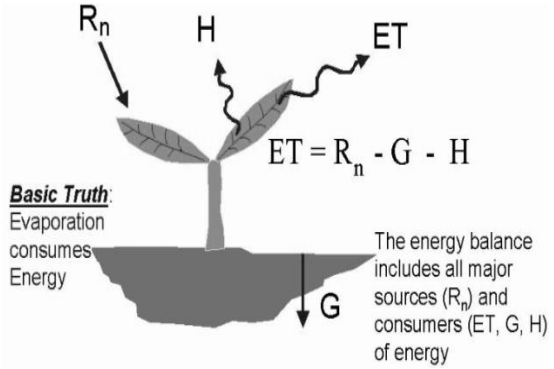

Figure 4 : Surface Energy Balance

The net radiation flux at the surface (Rn) represents the actual radiant energy available at the surface. It is computed by subtracting all outgoing radiant fluxes

from all incoming radiant fluxes. This is given in the surface radiation balance equation:

$$R_n = (R_s \downarrow - R_s \uparrow) + (R_L \downarrow - R_L \uparrow)$$

The first part of the equation (Rs↓ - Rs↑) represents the net shortwave radiation and the second part (RL↓ - RL↑) represents the net longwave radiation. Further representation of the equation is as follows:

$$R_n = (1-\alpha)R_s \downarrow + \varepsilon_a \sigma T_a^4 - \varepsilon_s \sigma T_s^4$$

Where; RS↓ is the incoming shortwave radiation (W/m^{-2}) which was measured at the Tono weather station, α is the surface albedo, σ is Stafan Boltzmann constant given as $5.67x10^{-8}Wm^{-2}K^{-1}$, ε_a is the emissivity of air described by Campbell and Norman (1998) as: $1.2x10^{-6}x(T_a+273.15)^2$, T_a is air temperature at the reference height, ε_s is surface emissivity and T_s is surface temperature.

B. Soil Heat Flux (G)

The relationship for soil heat flux is expressed as:

$$G = R_n\left[\Gamma_c + (1-f_c)(\Gamma_s - \Gamma_c)\right]$$

Where Γ_c= 0.05 for full vegetation canopy by Monteith cited in Su et al., (2001) and Γ_s= 0.315 for bare soil (Kustas and Daughtry, 1989)

C. Sensible Heat Flux (H)

The sensible heat flux derived in the similarity theory above is limited by wet sensible heat flux H_{wet} and dry sensible heat flux H_{dry} in SEBS. The dry limit sensible heat flux is given by;

$$H_{dry} = R_n - G$$

This equation is possible when the latent heat (evaporation) is zero due to the limitation of soil moisture content. During wet limit, the evaporation is at the potential rate and limited only by the energy at the earth's surface. The sensible heat flux is then reduced by:

$$H_{wet} = R_n - G - \lambda E \approx 0$$

Also at the wet limit, the internal resistance r_i is zero, by definition. Using the property in the equation below

$$\lambda E = \frac{\Delta \times r_e \times (R_n - G) + \rho C_p \times (e_s - e)}{r_e \times (\gamma + \Delta) + \gamma \times r_i}$$

and changing the subscript corresponding to the reflect the wet-limit condition, the sensible heat flux at the wet limit is given by:

$$H_{wet} = \frac{\left[(R_n - G) - \left(\frac{\rho C_p (e_s - e_a)}{r_{ew}\gamma}\right)\right]}{\left(1 + \frac{\Delta}{\gamma}\right)}$$

Where e_a is the actual vapour pressure measured, e_s is saturated vapour pressure derived in equation 28, γ is the Psychrometric constant, Δ is the rate of change of saturated vapour pressure with temperature and r_{ew} is the external resistance which is expressed as:

$$r_{ew} = \frac{1}{ku_*}\left[In\left(\frac{Z-d}{Z_{oh}}\right) - \Psi_h\left(\frac{Z-d}{L_w}\right) + \Psi_h\left(\frac{Z_{oh}}{L_w}\right)\right]$$

The above equation depends on the Obukhov length at the wet limit which is given by:

$$L_w = \frac{-\rho u_*^3}{\frac{kg \times 0.61 \times (R_n - G)}{\lambda}}$$

λ is the latent heat of vaporization= $2.45MJkg^{-1}$

The same procedure of the determination of sensible heat flux follows wet limit from equation 33 and 37 in iterative way.

According to Su, 2002, the Evaporative fraction is estimated as:

$$R_n = \lambda E + H + G$$

$$H_{dry} = R_n - G$$

$$H_{wet} = R_n - G - \lambda E_{wet} \approx 0$$

To derive the formula for relative evaporative expressed as:

$$\Lambda_r = \frac{\lambda E}{\lambda E_{wet}} = 1 - \frac{\lambda E_{wet} - \lambda E}{\lambda E_{wet}} = 1 - \frac{H - H_{wet}}{H_{dry} - H_{wet}}$$

The evaporative fraction is then expressed as:

$$\Lambda = \frac{\lambda E}{R_n - G} = \frac{\Lambda_r \lambda E_{wet}}{R_n - G}$$

When the evaporative fraction is known, the daily evaporation can be determined as:

$$E_{daily} = 8.64 \times 10^7 \times \Lambda \times \frac{R_{n*} - G_*}{\lambda \rho_w}$$

Where E_{daily} is the daily actual evaporation(mmd^{-1}), Л is the daily average evaporation fraction which can be approximated by SEBS estimate since the evaporative fraction is conservative(Shuttleworth et al., 1989; Sugita and Brutsaert, 1991; Crago, 1996), R_{n*} and G_* are the daily net radiation flux and soil heat flux and ρ_w is the density of water. The daily soil heat flux is close to zero because of the downward flux in daytime and upward flux at night balance each other approximately; the daily evaporation only depends on the net radiation flux given by:

$$R_{n*} = (1-\alpha)R\downarrow + \varepsilon L$$

Where R↓ is the daily incoming global radiation and L is the daily net longwave radiation.

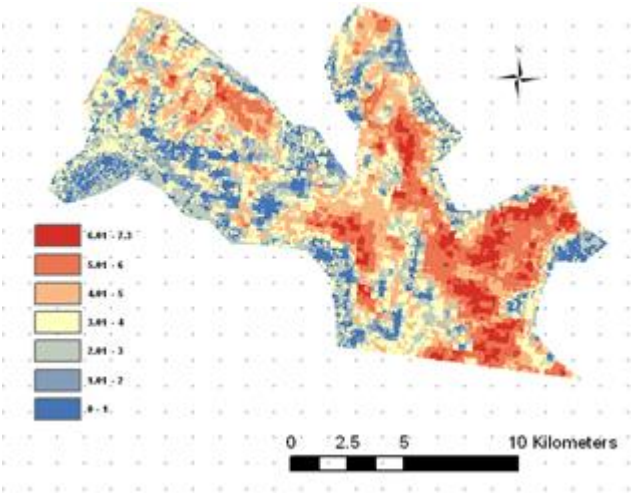

Figure 5 : Map of monthly actual evapotranspiration (January, 2009) of the study area

Estimation of Reference Evapotranspiration

According to Allen et. Al., 1998, the general form of Pernman Monteith equation is given as:

$$\lambda ET = \frac{\Delta(R_n - G) + \rho_a C_p \dfrac{(e_s - e_a)}{r_a}}{\Delta + \gamma\left(1 + \dfrac{r_s}{r_a}\right)}$$

where ET is evapotranspiration, Rn is the net radiation, G is the soil heat flux, (es-ea) is the vapour pressure deficit of the air, γ is the Psychrometric constant, Δ is the slope of the vapour pressure curve, λ is the latent heat of vaporization, cp is the specific heat of moist air at constant pressure, ρ is the air density, ra is the aerodynamic resistance to turbulent heat and vapor transfer, rc is the surface resistance. This equation can be applied to different vegetation and soil moisture conditions. By defining the reference crop as a actively growing and well watered green grass surface with a height of 0.12 m having a surface resistance of $70sm^{-1}$ and an albedo of 0.23, the FAO Penman-Monteith method to estimate ETo can be derived as (Allen et al., 1998):

$$ET_o = \frac{0.408\Delta(R_n - G) + \gamma\left(\dfrac{900}{T} + 273\right)u_2(e_s - e_a)}{\Delta + \gamma(1 + 0.34u_2}$$

Where: ET_o= Reference crop evaporation ($mmday^{-1}$)

R_n = Net radiation at the crop surface ($MJm^{-2}day^{-1}$)

G = Soil heat flux density ($MJm^{-2}day^{-1}$)

T = Mean daily air temperature at 2m height (°C)

U_2= Wind speed at 2m height (ms^{-1})

e_s = Saturated vapour pressure (kPa)

e_a = Actual vapour pressure (kPa)

$e_s - e_a$ = Saturated vapour pressure deficit (kPa)

Δ = Slope vapour pressure curve ($kPa°C^{-1}$)

γ = Psychrometric constant ($kPa°C^{-1}$)

To ensure the integrity of computations, the weather measurements should be made at 2 m (or converted to that height) above an extensive surface of green grass, shading the ground and not short of water.

III. RESULT AND DISCUSSION

The table and the figures below show the estimated climatic parameters and correlation analysis from Su et al., 2001 algorithm and Penman Monteith method during wet and dry seasons at Tono irrigation area.

Actual evapotranspiration (ET_a) is dependent of the precipitation. This implies that a change in precipitation is associated with ET_a. Actual evapotranspiration is an

important parameter for assessing the rate of transpiration in vegetation. It has a great impact on photosynthetic activity at the vegetation surface (NDVI). It is dependent on the unsaturated moisture storage properties of the soil, and affected by vegetated factors such as plant type and stage of growth (Freeze and Cherry, 1979)

The hydrological balance of ET_a and ET_o is shown in figure 4 below. The result showed that at the pick of the rainy season where there is abundant of moisture in the soil, ET_a rate equal ET_o, when the moisture content in the soil is limited as a result of insufficient rainfall and the crops unable to absorb water from the soil the ET_a becomes less than ET_o.

ET_a also showed negative correlation with ET_o and the surface temperature, which implies that during high surface temperature there is evapotranspiration of water from the soil creating water deficit around the root zone of the crops. This condition requires irrigation to supplement the insufficient rainfall (October to April). The hydrological balance of ET_o and precipitation is presented in figure 4. It showed from the results that from January to April and October to December ETo were higher than precipitation. This implies that irrigation was necessary to grow crops during these periods of non-availability of sufficient amount of precipitation and high atmospheric evaporative demand by crops. Also from April to October; precipitation was much higher than ETo, which could be the optimum planting date of crops. There was abundant supply of precipitation during these periods and might cause sudden flood if irrigation is not well- regulated. Moreover, figure 5 also showed the part of the rainfall which was effectively used by the crop after rainfall losses due to surface runoff and deep percolation. The effective rainfall is the rainfall ultimately used to determine the crop irrigation requirements.

TABLE I: Description of Aster satellite imageries used in the study

Aster	Bands	Resolution
Visible	2	15
Near infrared	7+1	30
Thermal infrared	5	60

TABLE III: Selected measured and estimated climatic parameters of the study area

Month	DOY	ET_a	ET_o
		mm/day	mm/day
January	16	2.30	5.80
February	47	2.30	6.43
March	75	2.78	6.30
April	106	3.01	6.50
May	136	3.45	6.15
June	167	3.50	5.55
July	197	3.95	4.45
August	228	4.38	4.47
September	259	3.78	5.01
October	289	2.90	5.58
November	320	2.70	5.54
December	350	2.50	5.44

TABLE II: Continuation

Month	Ppt.	Eff. ppt	S. Temp.
	mm	mm	^oC
January	0.00	0.00	43
February	0.00	0.00	42
March	0.00	0.00	40
April	30.30	28.80	39
May	125.10	100.10	39
June	131.10	103.60	38
July	176.90	126.80	36
August	289.30	153.90	33
September	155.90	117.00	36
October	4.20	4.20	39
November	0.00	0.00	39
December	0.00	0.00	40

Ppt. = precipitation, Eff. Ppt= effective precipitation, S. Temp. = Surface Temperature

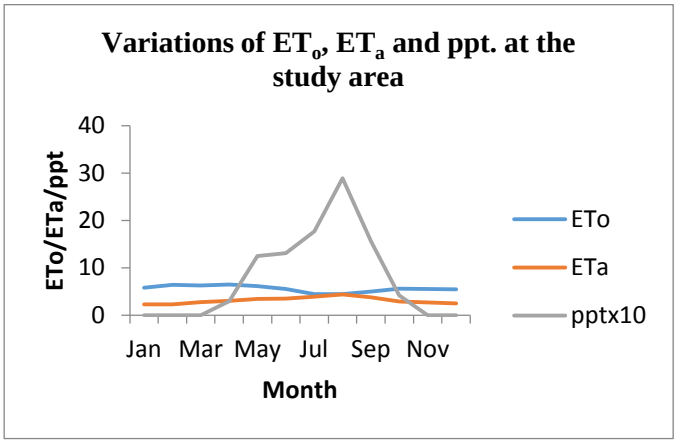

Figure 6: Variations of ET_o, ET_a and ppt at Tono Irrigation area

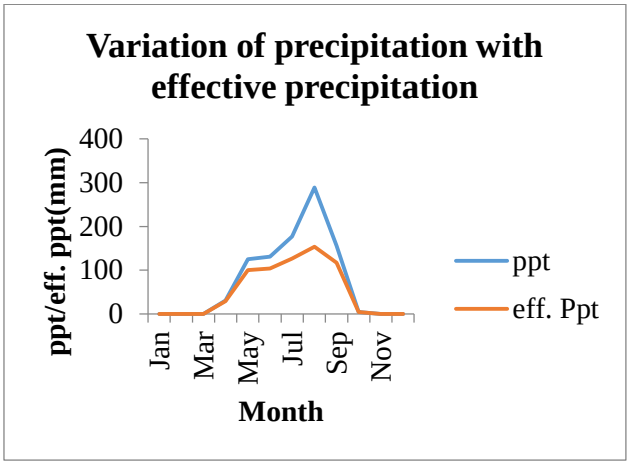

Figure 7: Variation of precipitation with effective precipitation

IV. CONCLUSION

Evapotranspiration is a major climatic parameter which plays important role in the hydrological cycle. This study presents analysis of the results of daily actual evapotranspiration obtained through SEBS algorithm and in comparison with reference evapotranspiration estimated from FAO Penman Monteith method and precipitation. The results showed that at the pick of the rainy season (August) where there is abundant moisture in the soil, ET_a rate is equal to ET_o. The ET_a becomes less in the dry season when there is a limited amount of moisture in the soil. The analysis of the result also showed that from January to April and October to December ETo were higher than precipitation. This implies that irrigation was necessary to grow crops during these periods of non-availability of sufficient amount of precipitation and high atmospheric evaporative demand by crops. Also from April to October; precipitation was much higher than ETo. There was abundant supply of precipitation during these periods and might cause sudden flood.

V. REFERENCES

[1] Allen R.G, Pereira L.S, Raes D, and Smith M., Crop evapotranspiration, guidelines for computing crop water requirements, 1986, FAO irrigation and Drainage paper 56, pp. 300, Rome, Italy

[2] Bouwer, L.M., Biggs, T.W., Aerts, C.J.H. Estimates of spatial variation in evaporation using satellite-derived surface temperature and a water balance model. Hydrological Processes, 2008, V. 22, p. 670 – 682.

[3] Brutsaert W., Aspect of bulk atmospheric boundary layer similarity under free convective conditions. Reviews of Geophysics, 1999, 37(4): 436-451

[4] Budyko, M. I. Climate and Life, 1974, Academic Press: Orlando.

[5] Campbell, G.S. And Norman, J.M., Introduction to environmental biophysics, 1998, Springer, New York 286pp

[6] Choudbury, B.J, Ahmed N.U, Idso S.B, Reginato R.J, and Daughtry C.S.T. Relations between evaporative coefficients and vegetation indices studied by model stimulations, 1994, Remote sensing of Environment, 50(1): 1-17

[7] Crago, R.D., Comparison of the evaporative fraction and the Priestley-Taylor α for parameterizing daytime evaporation, Water Resources Research. (1996) ISSN NO:0043-1397 DOI: 10.1029/96WR00269.

[8] Freeze, R.A., and Cherry, J.A., Groundwater, 1979: Englewood Cliffs, NJ, Prentice-Hall, 604 p.

[9] Gao, Y., Long, D., Li, Z. Estimation of daily evapotranspiration from remotely sensed data under complex terrain over the upper Chao river basin in North China, 2008, International Journal of Remote Sensing, V. 29, No. 11, p. 3295 – 3315.

[10] Gordon, L., Dunlop, M., Foran, B. Land cover change and water vapour flows: learning from Australia, 2003, Philosophical Transactions of the Royal Society of London, Series B: Biological Sciences, v. 358, p. 1973–1984.

[11] Kustas W.P and Daughtry S.T. Estimation of the soil heat flux-net radiation radio from spectra data,

1989, In Agricultural and Forest Meteorology, 49(1990), pp. 205-223
[12] Liang S. Narrowband conversions of land surface albedo 1: Algorithms, 2000, Remote Sensing of Environment 84(1): pp. 25-41
[13] Milly, P. C. D., Dunne, K. A. Trends in evaporation and surface cooling in the Mississippi River basin, 2001, Geophysical Research Letters, v. 28, p. 1219–1222.
[14] Rahman H and Dedieu G. SMAC: a simplified method for the atmospheric correction of satellite measurements in the solar spectrum, 1994, International Journal of Remote Sensing, Vol. 15, No. 1: 123-143
[15] Shuttleworth, W. J., Micrometeorology of tropical and temperate forest, 1989, Phil. Trans. Roy. Soc. Lond., B324, 299-334
[16] Smith M. CROPWAT: Manual and Guidelines, 1991, FAO of UN, Rome.
[17] Su Z and Jacobs C. ENVISAT: actual evaporation. BCRS Report 2001: USP-2 report 2001. Publication of National Remote Sensing Board, Delft, pp. 57.
[18] Su Z., The surface energy balance system for estimation of Turbulent heat flux, 2002, Hydrological and Earth System Sciences, 6(1): 85-89
[19] Sugita, M. and Brutsaert, W., Daily evaporation over a region from lower boundary layer profiles measured with radiosondes, 1991,Water Resource Research., 27(10), 747–752.
[20] Valor E and Caselles V., Mapping land surface emissivity from NDVI, 1996, Application to European, African and South American areas. Remote Sensing of Environment 57(3): 167-184